Imaging the dynamics of magma propagation using radiated seismic intensity.

B. Taisne, Florent Brenguier, N.M. Shapiro, Valérie Ferrazzini

Imaging the dynamics of magma propagation using radiated seismic intensity

B. Taisne,[1] F. Brenguier,[1,2] N.M. Shapiro,[1] and V. Ferrazzini[2,3]

[1]Department of Seismology, Institut de Physique du Globe de Paris, Sorbonne Paris Cité, CNRS (UMR7154), 1 rue Jussieu, 75238 Paris, cedex 5, France.

[2]Observatoire Volcanologique du Piton de la Fournaise, Institut de Physique du Globe de Paris, Sorbonne Paris Cité, CNRS (UMR7154), 14RN3 - Km 27, 97418 La Plaine des Cafres, La Réunion, France.

[3]Géologie des systèmes volcaniques, Institut de Physique du Globe de Paris, Sorbonne Paris Cité, CNRS (UMR7154), 1 rue Jussieu, 75238 Paris, cedex 5, France.

At shallow depth beneath Earth's surface, magma propagates through strongly heterogeneous volcanic material. Inversion of buoyancy and/or solidification have strong impacts on the dynamics of propagation without any change of magma supply. In this paper, we study the spatial and time evolution of magma intrusions using induced seismicity. We propose a new method based on estimates of radiated seismic intensities recorded at different stations during seismic swarms at Piton de la Fournaise volcano. By applying this method to the January 2010 Piton de la Fournaise volcano eruption, we image complex dike propagation dynamics which strongly differ from a model of constant velocity dike propagation. We provide a new and fully automatic method to image in real time the dynamics of dike propagation and to infer the position of eruptive fissures.

1. Introduction

Eruption precursory activity associated to volcanic unrest is currently recorded at many volcanological observatories around the world and mainly consists of seismicity and ground deformation monitoring. During magma propagation to the near-surface, the vicinity of the associated dike or sill is subjected to a large stress field perturbation [*Rubin and Gillard*, 1998], that will concentrate most of the induced seismicity (seismic swarms). Monitoring these seismic swarms is thus a potentially powerful technique to track magma movements but is not used to its full potential for several reasons. During seismic swarms, seismic events are difficult to separate, so that one may not use the efficient localization methods that have been devised for single earthquakes. Only those events that are well identified can be treated with current methods and a large part of the seismic signal is left unused. Consequently, the interpretation of the data in term of the dynamics of magma migration is difficult. Previously, few examples of migration of seismicity associated with magma movement have been imaged by geophyscial means [*Aoki et al.*, 1999; *Hayashi and Morita*, 2003; *Battaglia et al.*, 2005]. However, precise analysis of seismicity (localization, magnitude) requires post-processing and is therefore difficult to perform in real time.

Here, we propose a simple but robust method to track magma movements using the ratio at different seismic stations of the seismic intensities radiated by the surroundings of the dike's tip. We apply this method to the January 2010 eruption of Piton de la Fournaise volcano (La Réunion island). As a result, we observe a complex dike propagation dynamic which strongly differs from a model of constant velocity dike propagation. We thus provide

a fully automatic and simple method to image in near-real time the dynamics of dike propagation and to infer the position of eruptive fissures.

2. Method

Traditionally, seismic events are located using P or S wave travel time delays measured at different receivers. This approach finds its limits when it becomes difficult to measure accurate arrival times such as for example, during seismic swarms or in cases of low signal to noise ratio micro-seismicity. Here, we propose a method to automatically estimate the position at depth of a seismic source by using the differences in seismic amplitudes recorded at difference sensors. This approach relies on the attenuation of seismic waves along the source-receiver travel path. In order to avoid the detection of single P or S wave arrivals, we use an estimate of the average recorded seismic intensity over a time window much longer than the seismic wave travel time delays at different sensors (see section 3 for details). Following *Battaglia and Aki* [2003], we use a simple attenuation law that takes into account geometrical and intrensic but not scattering attenuation (equation 1).

$$I_i = A_o \frac{e^{-Br_i}}{r_i^n}\,, \tag{1}$$

with,

$$B = \frac{\pi f}{Q\beta}\,, \tag{2}$$

where I_i is the seismic intensity recorded at receiver i, r_i is the distance from the source, I_o is the source radiated seismic intensity, f is frequency, β is shear wave velocity and Q is the quality factor for attenuation. The index $n = 1$ for body waves and $n = 0.5$ for surface waves. For simplification we consider an isotropic medium with constant B. Because we

don't know which type of wave (body or surface) dominates the intensity estimates, we make no approximation about the value of n. In the next section we will investigate the effect of n and Q.

To avoid the estimate of the seismic intensity at the source (I_o), we choose to analyse the ratios of seismic intensities between all sensors (equation 3) rather than the true seismic intensities at different sensors.

$$\left.\frac{I_i}{I_j}\right|^t = \left(\frac{r_j^t}{r_i^t}\right)^n \exp\left[-B(r_i^t - r_j^t)\right] \ . \tag{3}$$

Assuming a migration such that $r_i^{t+\delta t} = r_i^t + \delta_i$ and $r_j^{t+\delta t} = r_j^t + \delta_j$, with δ_i and δ_j that can be defined either positively or negatively depending on the relative direction of the source to the station:

$$\left.\frac{I_i}{I_j}\right|^{t+\delta t} = \left(\frac{r_j^t + \delta_j}{r_i^t + \delta_i}\right)^n \exp\left[-B(r_i^t + \delta_i - r_j^t - \delta_j)\right] \ , \tag{4}$$

by first order linearisation we obtain :

$$\left.\frac{I_i}{I_j}\right|^{t+\delta t} = \left.\frac{A_i}{A_j}\right|^t \left[1 + \delta_j\left(\frac{n}{r_j^t} + B\right) - \delta_i\left(\frac{n}{r_i^t} + B\right)\right] \ . \tag{5}$$

Equation 5 shows that only the migration of seismicity will affect the intensity ratio and not the change of radiated seismic intensity at the source which does not appear in the final equation. The only exception is if the motion occurs within the plane perpendicular to the middle of the line defined by the two stations. In this particular case the intensity ratio will remain unchanged. For the present purpose, and using the fact that we use different stations, we will consider any temporal changes as a result of the migration of the seismic source and therefore to the migration of the magma.

3. Example of data processing

As an application of the proposed method, we focus on Piton de la Fournaise (PdF) volcano located on La Réunion island in the Indian ocean (Figure 1). It is a basaltic shield volcano which erupted more than 30 times between 2000 and 2010. Since 2009-2010, 15 broad-band seismic stations have been installed on the volcano as part of the UnderVolc project, in addition to the existing seismic array. We analyse data from the 2010 January euruption. The selected eruption presents a seismic swarm that can be divided into two phases (figure 2 a and b). During the first phase, which lasted for about an hour, a high level of seismicity was recorded followed by a relatively quiet phase that directly precede the onset of the eruption (seismic tremor).

As a first stage of data processing we correct the signal from the sensor and acquisition sensitivity to retrieve accurate values of ground motion velocity. Seismic signal amplitudes have also been corrected from site effects using the coda amplification factor method [*Battaglia and Aki*, 2003].

Seismicity induced by magma migration presents a relatively high frequency content compared to the permanent back-ground noise. For this study we will only consider a frequency range between 5Hz and 15Hz.

We calculate the envelope of the signal, E, using the norm between the filtered data, x, and their Hilbert transform, H:

$$E = \sqrt{(H(x) - x)^2} \ . \tag{6}$$

To eliminate spikes or glitches we decimate the data by keeping the median of 1000 consecutive points, corresponding to 10 seconds. This leads to the seismic intensity estimate, I, that we will use from now.

The last step of the analysis is a median filter applied on I using a sliding window of given duration Δt.

The nomenclature used is :

$$I_{\mathrm{Sta}}^{\Delta t}\,, \tag{7}$$

with Sta corresponding to the name of the station. Figure 2 c and d represents the results of this data processing for $\Delta t = 5min$.

To highlight relative changes of intensity between different stations we plot the ratio $I_{\mathrm{Sta}_1}^{\Delta t}/I_{\mathrm{Sta}_2}^{\Delta t}$ (one example is shown figure 2 e).

4. Results

Ratios for different pairs of stations are shown figure 3 a. It is important to note that since this method relies on the seismo-acoustic emmissions from the dike's tip, we only show results corresponding to periods when signal intensities $I_{Sta}^{\Delta_t}$ are at least twice the background seismic noise intensity level.

We also compare observations of intensity ratios to synthetic itensity ratios at station UV05 and FLR (figure 3 b and c) using a theoretical vertical pathway beneath the eruptive vent and a constant propagation velocity from sea level (0 meters a.s.l at 07:54 AM) to the surface (2500 m at 10:25 AM). The intensity ratios are calculated using equation 3 for different value for the quality factor (Q) and both volumetric and surface attenuation (respectively $n = 1$ and $n = 0.5$). An interesting point is the behaviour of the theoretical

curve that presents an apparent acceleration since the migration is set to be at constant speed.

Interestingly the beginning of the seismic swarm (07:54 to 09:00 AM) shows a high level of seismicity with intensity ratios close to unity and with no significant variations which can be interpreted as a slow migration of the magma. In the later part of the seismic swarm (09:00 AM to 10:25 AM) seismic activity strongly decreases and intensity ratios show strong variations. This can be interpreted as a fast migration of the magma in the shallow part of the edifice. This migration presents some heterogeneity with a phase of arrest around 10:00 AM.

Simple modelling does not explain the temporal change of the intensity ratio and shows that simple migration is not likely to occur in natural systems. Nevertheless, the intensity ratio during the tremor can be explained using $n = 1$ and $Q \sim 200$, which does not seem a reasonable value for the quality factor, or using $n = 0.5$ and $Q \sim 50$, which implies that the computed seismic intensities are dominated by surface waves. This Q value is in agreement with previous studies [*Battaglia and Aki*, 2003; *Battaglia et al.*, 2005].

Regarding the ratio presented figure 3 a, the change at 10:09 AM could be due to a change in the direction of the propagation from vertical to horizontal toward station UV05. This highlights the need to develop an inverse problem to extract the position of the propagating front from all the possible intensity ratios.

5. Inverse problem

In order to image magma propagation at depth, we seek the best position within a grid that best explains the intensity ratios from all possible pairs of stations. We process a

simple inverse problem in which we compute all the theoretical intensity ratios on each point of the grid defined as follows: Easting from 362 km to 370 km every 100m, Northing from 7647 km to 7653 km every 100 m and depth from -0.5 km to 2.5 km above see level every 50 m. The limitation in depth comes from the localisation of individual events at the beginning of the seismic swarm. Parameters used for the attenuation law are $n = 0.5$ and $Q = 50$.

The 3-dimensional misfit used is the following :

$$\chi = \sqrt{\sum_i \sum_{j>i} \left(\frac{I^{\Delta t}_{\mathrm{Sta}_i}}{I^{\Delta t}_{\mathrm{Sta}_j}}\bigg|^{\mathrm{calculated}} - \frac{I^{\Delta t}_{\mathrm{Sta}_i}}{I^{\Delta t}_{\mathrm{Sta}_j}}\bigg|^{\mathrm{measured}} \right)^2} . \quad (8)$$

The results are shown figure 4. During the period of high seismic activity, locations are saturated at see level which is consistent with commonly observed seismicity on PdF volcano and the location of single events at the beginning of seismic swarms. As already observed in figure 3, the inversion results show a phase of arrest around 10:00 AM.

6. Discussions and Conclusions

The proposed analysis will find a limitation when the source of the seismicity is far from all the stations. In that case, the relative difference in the source-receiver paths are negligible and all the possible intensity ratios will be close to one. This also implies, for future inversion of the migration using intensity ratios, that the error on the position will be a function of the position itself: the greater the source-receiver distance, the greater the error will be.

In term of the dynamics of magma propagation, the results clearly show that the upward migration started between 9:00 AM and 9:30 AM. Combining intensity ratios (figure 3) and the results of the inversion (figure 4) we can infer that the migration initiates at 9:00 AM with clear migration toward the surface at 9:25 AM which corresponds to about one hour after the beginning of the seimic swarm. At smaller scale the upward propagation does not occur at constant velocity but presents phases of rapid propagation and phases of arrest or with a strong decrease of velocity.

This simple analysis can be easily applied to the real time monitoring of magma migration and gives an opportunity to extract information on the dynamics of magma propagation.

Acknowledgments. The data used for the analysis were collected by the Institut de Physique du Globe de Paris, Observatoire Volcanologique du Piton de la Fournaise (IPGP/OVPF) and the Laboratoire de Gèophysique Interne et Tectonophysique (LGIT) within the framework of ANR_08_RISK_011/UnderVolc project. The sensors are properties of the réseau sismologique mobile Français, Sismob (INSU-CNRS). We are grateful to Daniel Clarke for fruitful comments about the manuscript. This work has been supported by ANR (France) under contracts 05-CATT-010-01 (PRECORSIS), ANR-06-CEXC-005 (COHERSIS), ANR-08-RISK-011 (UNDERVOLC) and by a FP7 European Research Council advanced grant 227507 (WHISPER). This is IPGP contribution number XXXX.

References

Aoki, Y., P. Segall, T. Kato, P. Cervelli, and S. Shimada, Imaging magma transport during the 1997 seismic swarm off the Izu Peninsula, Japan, *Science*, *286*, 927–930, 1999.

Battaglia, J., and K. Aki, Location of seismic events and eruptive fissures on the Piton de la Fournaise volcano using seismic amplitudes, *J. Geophys. Res.*, *108*, 2364, doi: 10.1029/2002JB002193, 2003.

Battaglia, J., K. Aki, and V. Ferrazzini, Location of tremor sources and estimation of lava output using tremor source amplitude on the Piton de la Fournaise volcano: 1. Location of tremor sources, *Journal of Volcanology and Geothermal Research*, *147*, 268–290, doi: 10.1016/j.jvolgeores.2005.04.005, 2005.

Battaglia, J., V. Ferrazzini, T. Staudacher, K. Aki, and J.-L. Cheminée, Pre-eruptive migration of earthquakes at the Piton de la Fournaise volcano (Réunion Island), *Geophys. J. Int.*, *161*, 549–558, 2005.

Hayashi, Y., and Y. Morita, An image of magma intrusion process inferred from precise hypocentral migration of the earthquake swarm east of the Izu Peninsula, *Geophys. J. Int.*, *153*, 159–174, 2003.

Rubin, A. M., and D. Gillard, Dike-induced earthquakes: Theoretical considerations, *J. Geophys. Res.*, *103*, 10,017–10,030, 1998.

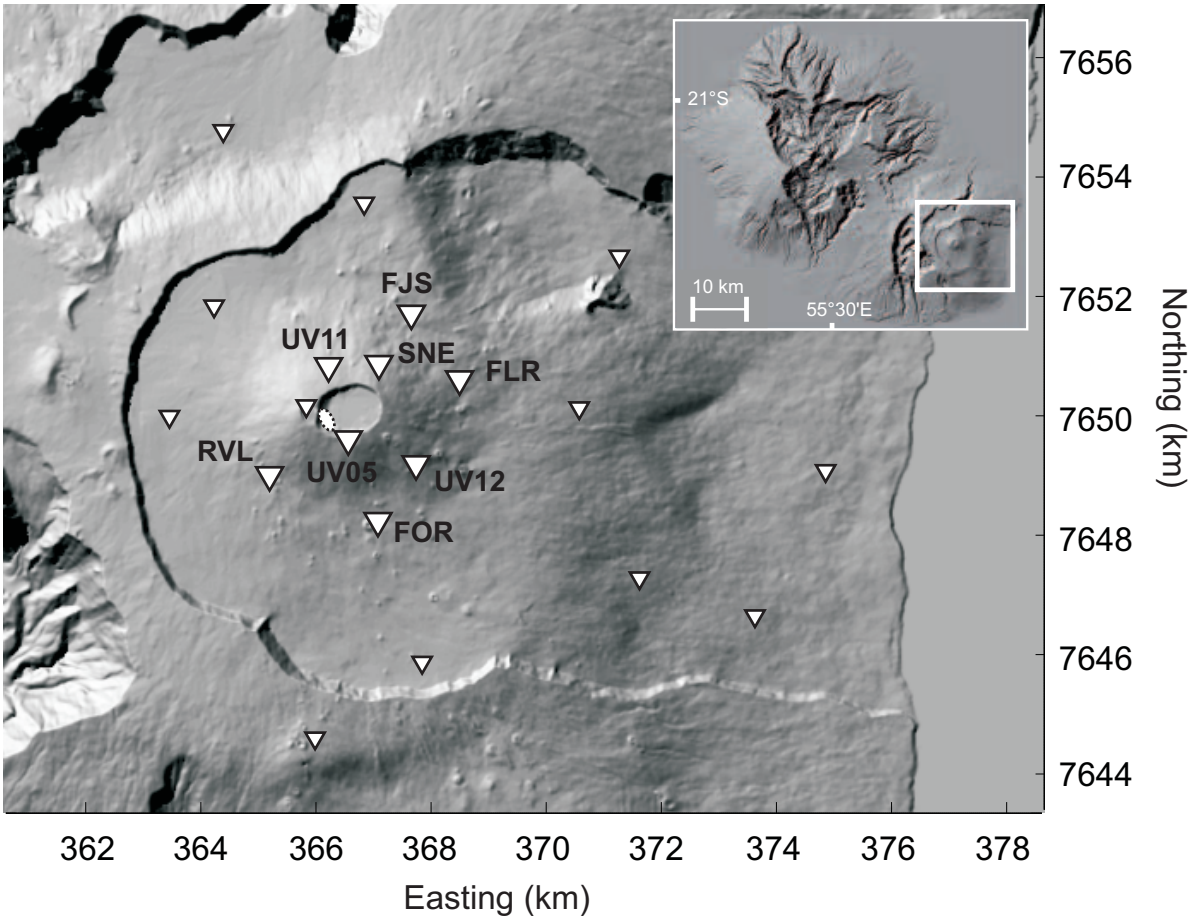

Figure 1. Location of Piton de la Fournaise volcano on La Réunion island (inset) and seismic station distribution (inverted triangles). Those used in this study are referred by their names on the map. The position of the January 2010 eruptive fissure is shown as a dashed circle.

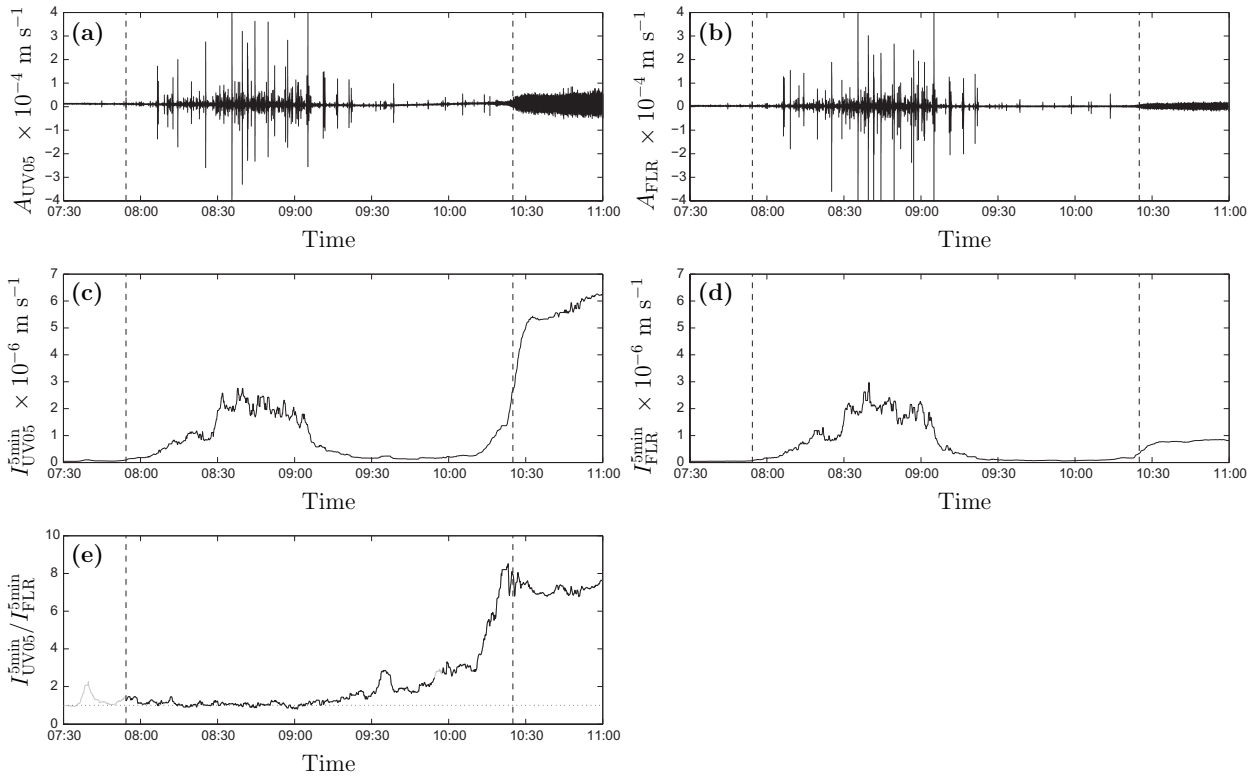

Figure 2. Example of data processing. **a** and **b** represent the raw ground velocity at stations UV05 and FLR respectively. **c** and **d** represent the seismic intensities, see section 3 for further details. **e** represents the ratio between $I^{5\text{min}}_{\text{UV05}}$ and $I^{5\text{min}}_{\text{FLR}}$. Vertical dashed lines represent the beginning of the seismic swarm (07:54 AM) and the onset of the eruption (10:25 AM).

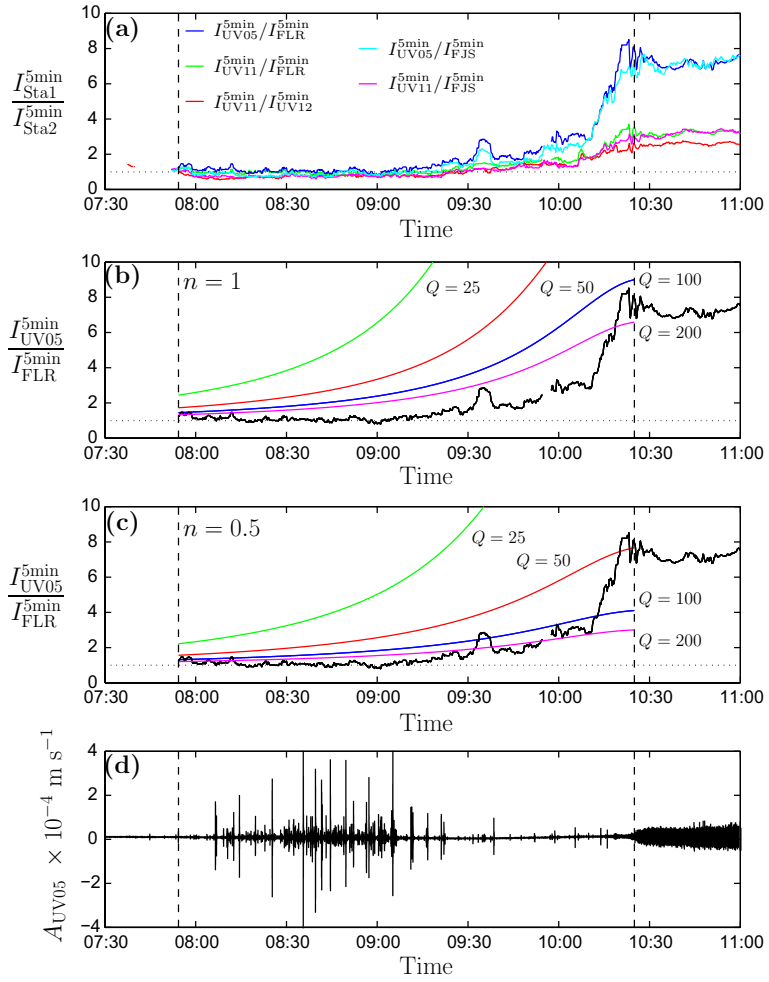

Figure 3. **a**, Seismic intensity ratio for five different station pairs ($\Delta t = 5min$). Comparison of real and synthetic ratios for station pair UV05, FLR using different quality factors and considering body wave (**b**) or surface wave (**c**) attenuation (respectively, $n = 1$ and $n = 0.5$). The synthetic curves are calculated for a source migrating at constant vertical velocity from sea level at 07:54 AM to the vent at 10:25 AM. **d** represents the raw seismic signal at station UV05 for timing comparison. Vertical dashed lines represent the beginning of the seismic swarm (07:54 AM) and the onset of the eruption (10:25 AM).

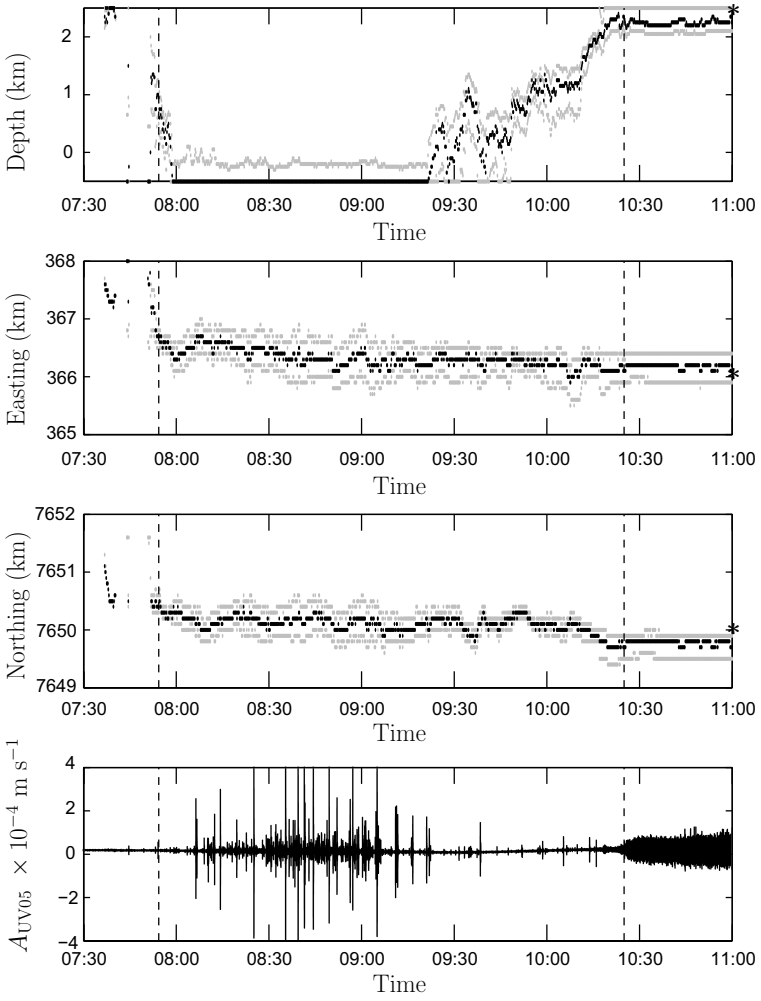

Figure 4. Inversion results. The top three panels show the results of the inversion in terms of depth (above sea level), Easting and Northing. For each component, the black curve represents the best position of the minimum misfit and both grey curve represent the minimum and maximum extension of a volume including misfit values inferior to 10% of the minimum misfit. The bottom panel represents the seismic signal at station UV05 for timing comparison. Vertical dashed lines represent the beginning of the seismic swarm (07:54 AM) and the onset of the eruption (10:25 AM). The black stars show the location of the eruptive fissure.